Influence of a Few Short Branches on the Amorphous Region of a Semicrystalline Polymer: Simulation on a Cubic Lattice

Saubhagya C. Mathur, Klein Rodrigues, and Wayne L. Mattice*

Institute of Polymer Science, The University of Akron, Akron, Ohio 44325.
Received September 22, 1988; Revised Manuscript Received December 14, 1988

ABSTRACT: A recent study of the amorphous region between two crystalline lamellae on a two-dimensional square lattice has been extended to a three-dimensional cubic lattice. A system without short branches has been used as a reference. The systems with short branches have ~1–2% of the lattice sites occupied by trifunctional branch points. Each individual branch occupies one or two lattice sites. The more dramatic effects are seen in the presence of the longer of the two short branches, and these effects are localized in those layers that are close to the crystal–amorphous boundary. The anisotropic interfacial region, located between the crystal and the truly isotropic region, shows an increase in size with an increase in content of the larger of the two short branches. The nonuniform distribution of these branches observed in the two-dimensional simulations persists when the simulations are performed in three dimensions. The smaller of the two short branches shows a lower tendency for segregation. The fraction of tie chains increases slightly in the presence of branches that each occupy two lattice sites. Zeroth-order tight folds also increase, but adjacent reentrant loops (other than zeroth-order tight folds) decrease. Entanglements of loops originating from opposite crystal faces seem to be unaffected by the incorporation of branches.

Introduction

Copolymers of ethylene and a 1-alkene have become enormously important during the last decade. The primary reason for the interest in these copolymers is the range of properties achievable by the selection of the type and amount of 1-alkene used as the comonomer in the polymerization. The copolymers have higher tensile and tear strengths than the conventional low-density polyethylene obtained from free-radical polymerization.[1] The structural feature that distinguishes these copolymers from the conventional low-density polyethylene is the type of branches. The conventional material has both long and short branches present,[2,3] and the short branches are of various types.[4–6] On the other hand, the copolymers contain no long branches, and the short branches are of uniform type because they arise from the 1-alkene comonomer.

Studies of the conformational properties of chain segments that lie in the amorphous regions between two crystalline lamellae have been undertaken to obtain a rational explanation of the dependence of the bulk properties on the number and type of short branches.[7,8] These previous studies utilized two methods that differ in their attention to intermolecular and intramolecular interactions. The first study[7] employed a simple method involving the combination of the characteristic ratio for the branched chain with the analytical results to the Gambler's ruin problem.[9–11] The strengths of this approach were its mathematical simplicity and its ability to incorporate, in exquisite detail, the influence of intrachain interactions on the chain conformation. Its weaknesses (which are fatal[8]) are the inability to take into account any tendency for segregation of short branches within the amorphous region or the special interchain interactions that are found in the anisotropic interfacial region that exists between the crystal and the isotropic region. The former of these two weaknesses is unique to lightly branched copolymers, but the latter weakness occurs in homopolymers as well.

The second study[8] was a simulation of the amorphous region on a square lattice in which every site is singly occupied. This approach gives a less realistic account of the bond angles, dihedral angles, and short-range intramolecular interactions in a polyethylene chain, but it has the potential of providing information about conformational effects that arise from intermolecular interactions in the interfacial region. The marked tendency for segregation of the short branches in the anisotropic interfacial region and an accompanying growth in this interfacial region were both revealed in these simulations.[8] The observation in the simulations of a growth in the anisotropic interfacial region has its experimental counterpart in the analysis of the Raman internal modes by Alamo et al.[12] The segregation of the short branches in the simulations has its experimental counterpart in the recent neutron-scattering measurements with labeled ethylene–1-alkene copolymers by Stein and co-workers.[13]

A qualitative argument suggests that the nonuniform distribution of short branches on the square lattice should persist in three dimensions.[8] Here we report the results of the simulations on a cubic lattice and the verification of the qualitative prediction. Simulation on the three-dimensional cubic lattice also provides an opportunity for the investigation of the occurrence of entangled loops,[14–16] which are forbidden on the square lattice.

Simulation

Three different kinds of simulations were performed. The first one involved no short branches and was used as a reference. This simulation simply repeats the work of Mansfield.[17] In the other two kinds of simulations, short branches that each occupy one or two lattice sites are present. With the smaller branch, ~2% of the lattice sites was occupied by trifunctional branch points. Two simulations, in which ~1% and 2% of the lattice sites were occupied by trifunctional branch points, were performed with the larger branches. The chains and the branches were initially arranged in a regular array on a cubic lattice of size $7 \times 7 \times 30$ beads, where 30 beads are in the direction (z direction) normal to the crystal–amorphous boundary, and 7 beads are present in the x and y directions. The axis system is depicted in Figure 1. Periodic boundary conditions were employed in the directions x and y. The simulation procedure is identical with the one employed in the two-dimensional simulation in the previous study.[8] The various rearrangement moves and the algorithm are briefly described below for convenience. The detailed description can be found in ref 8.

For chain segments without branches, rearrangement is accomplished by bond flipping[17] with some added restrictions.[8] For the short branches, rearrangement is accomplished by end attack as well as simultaneous creation and destruction of branches.[8] All moves described for the

0024-9297/89/2222-2781$01.50/0

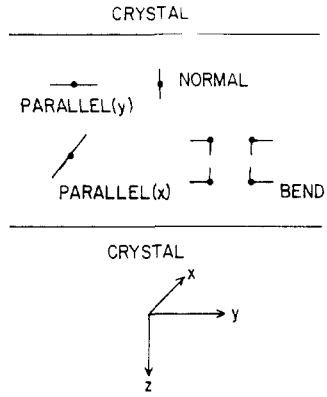

Figure 1. Various kinds of consecutive bond pairs and the coordinate system used.

two-dimensional simulation in the previous study[8] have been extended to three dimensions in the present study.

Each bead in the lattice was identified by a unique IDTAG, which was a positive integer calculated from the coordinate of the bead as $L_zL_yX + L_zY + Z + 1$. L_y and L_z are the lattice sizes in the y and z directions, respectively, and X, Y, and Z are the three coordinates of the bead. In the present simulation, $L_x = L_y = 7$ and $L_z = 30$ have been used. The maximum size of the lattice was chosen on the basis of computational limitations. The separation between the two crystal faces is the same as in the case of the two-dimensional simulation. The horizontal layers in the lattice were sequentially numbered 1–30 as one goes from the top layer to the bottom ($Z = 0$ to $Z = 29$). All the IDTAGs for the lattice were stored in a three-dimensional array KAR(I,J,K) with dimension $30 \times 7 \times 7$ for ease of location of any bead in the lattice. The chains and branches were stored in two-dimensional arrays IC(I,J) and IBR(I,J) in a fashion similar to the two-dimensional simulation. The interfacial beads (layers 1 and 30) were stored in another array ICR containing 98 beads.

The regions above layer 1 and below layer 30 were assumed to be crystalline regions, as before. By ignoring the regions above layer 1, and below layer 30, we tacitly assume that any stem can enter the crystalline region. The validity of this assumption deteriorates as the branch content increases. The present simulations show how the presence of short branches modifies the amorphous region when the branch content is low.

At the beginning of a move cycle, 1 of the 1470 beads in the lattice is randomly selected. If this bead is located on a branch, then an end attack is attempted. If the bead does not belong to a branch, then another bead is selected from the six coordinating beads. The bonds connected to the beads are located, and a bond flip is attempted. In the next step, a branch is selected at random, and simultaneous creation and destruction of a branch is attempted. The algorithm then returns to the beginning of the move cycle until the desired number of moves has been attempted.

The parameters of interest include all from the two-dimensional studies, such as the probabilities of ties (obtained in terms of fraction of chains that are ties), loops, tight folds, and adjacent reentry. Branch distribution and interfacial region were also investigated in a way similar to the previous study.[8] For the study of the interfacial region, there are now two kinds of parallel bond pairs (X and Y directions), as shown in Figure 1. In completely isotropic regions, the fraction of the normal bond pairs would be equal to those of the parallel bond pairs in the X direction and to the fraction of parallel bond pairs in the Y direction. An anisotropic interfacial region can be detected from lattice simulations by studying the variation of the fraction of these bond pairs as a function of the distance of the layer from the crystal–amorphous boundary. An increase in the fraction of normal bond pairs over the average of the two kinds of parallel bond pairs signifies the presence of an anisotropic interfacial region.

Table I
Ties, Loops, Tight Folds, and Adjacent Reentry

	unbranched		1% branches		2% branches	
	mean	σ^a	mean	σ	mean	σ
ties	2.5	0.1	2.5	0.1	2.8	0.2
loops	20.5	0.7	17.0	0.6	17.9	0.7
tight folds	77.0	0.7	80.5	0.6	79.4	0.6
adjacent reentry	6.0	0.5	2.4	0.3	2.7	0.3

[a] σ denotes the standard deviation of the mean.

The new parameter that was studied in the three-dimensional simulation is loop entanglement. The parameter is measured as the link density, which is defined as the fraction of loops originating from a particular crystal face that are entangled with at least one loop originating from the opposite crystal face. The average link density can be computed from the two link densities for the two crystal faces. The algorithm for computation of linking was adopted from the studies by Lacher et al.[14-16]

Results and Discussion

As was mentioned in the previous paper,[8] the branches that occupy one or two lattice sites should not be equated to methyl and ethyl branches due to the artificial restrictions imposed by the lattice on bond angles and dihedral angles.[18] However, the types of effects that can be expected upon a change in the size of the short branches can be illustrated from such simulations on lattices.

Ties, Loops, and Tight Folds. The effects produced by the incorporation of short branches that occupy two lattice sites are summarized in Table I. There is a suggestion that short branches may produce a slight increase in ties, but the increase is just at the edge of the standard deviation of the mean, which is also shown for all the parameters in this table. The fraction of tight folds is elevated slightly in the presence of short branches, and the fraction of adjacent reentrant loops that are not tight folds drops by almost the same amount. There is little change in the content of nonadjacent reentrant loops, and consequently the decrease in the content of loops is determined by the change in adjacent reentrant loops. Of course, the content of tight bends in all of the simulations would be reduced if energetic terms dictated by the short-range intramolecular interactions in polyethylene were incorporated in the simulations. The extent of the interfacial region, which is discussed in the next paragraph, will also be affected. Additional simulations will be required to determine the magnitude of these effects.

Bond Pairs. Interfacial Region. Figures 2–4 show the variation of the fraction of different kinds of bond pairs (see Figure 1) as a function of layer number for simulations without branches and with branches that occupy two lattice sites. The results have been averaged over layers equidistant from the two crystal–amorphous boundaries. Thus, values cited for layer i are the average of the value at layer i and layer $30 - (i - 1)$. First consider the bend bond pairs. These pairs in layer 1 (and layer 30) arise from zeroth-order tight folds. The probability for tight folds, and also the probability of bend pairs in layer 1, increases from 0.77 in the unbranched case to ~0.8 in the systems with 1% and 2% branch content. The branches cause a slight reduction in bend bond pairs in the next few layers.

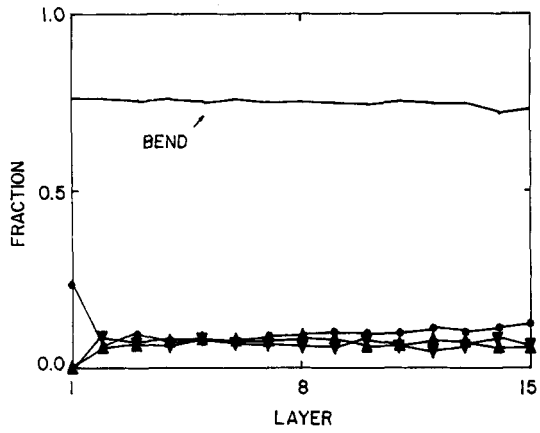

Figure 2. Variation in the different types of bond pairs with distance from the crystal–amorphous boundary (layer number) for the unbranched system. Normal, parallel (x), and parallel (y) bond pairs are denoted by ●, ▲, and ▼, respectively.

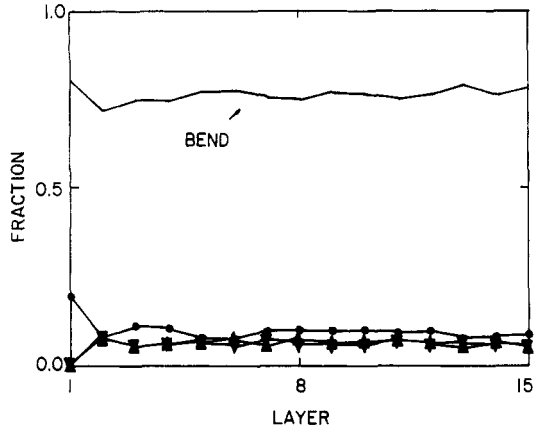

Figure 3. Same as Figure 2 for 1% branch content. Each branch occupies two lattice sites.

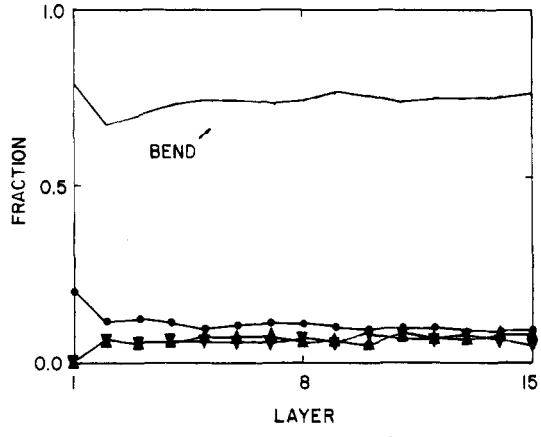

Figure 4. Same as Figure 3 for 2% branch content.

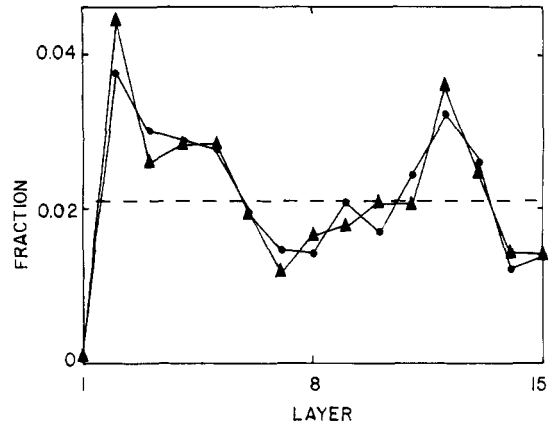

Figure 5. Variation in fraction of sites belonging to branch points (▲) and branch ends (●) as a function of layer number for 2% branch content. Each branch occupies one lattice site. The dashed line is the expectation for a random distribution of short branches.

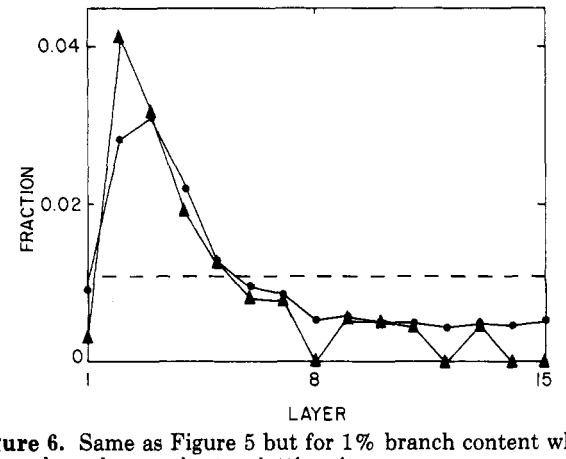

Figure 6. Same as Figure 5 but for 1% branch content when a short branch occupies two lattice sites.

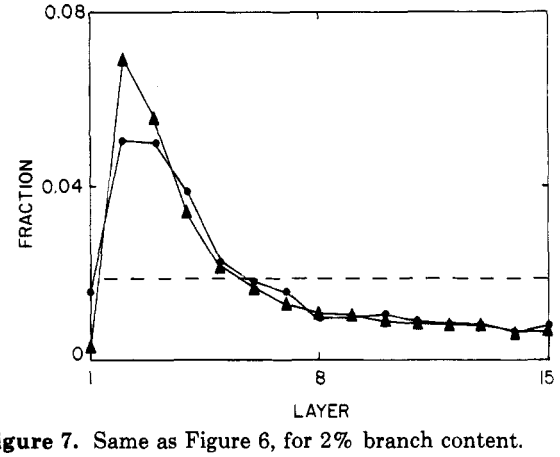

Figure 7. Same as Figure 6, for 2% branch content.

Beyond these layers, there is little indication of an influence of branching on the bend pairs.

For the unbranched system (Figure 2), the normal and parallel bond pairs are nearly equal at layer 2, indicating the absence of a significant interfacial region. Similar results for the unbranched system, in the absence of energetic terms, were obtained by Mansfield.[17] In the presence of 1% branches (Figure 3), the development of an interfacial region is suggested by an increase in the preference for normal bond pairs over parallel bond pairs in layers 3 and 4. The preference extends out to ~layer 10 when the branch content is increased to 2% (Figure 4). The increase in short branch content increases the penetration of the preference for normal bond pairs into the amorphous region, and it therefore increases the extent of the anisotropic interfacial region. Analysis of the Raman internal modes shows that the anisotropic interfacial region does indeed increase upon the incorporation of short branches in ethylene–1-alkene copolymers.[12]

Distribution of Branches. In the two-dimensional simulation, it was observed that the short branches, which each occupy two lattice sites, are not uniformly distributed throughout the amorphous region.[8] Instead they prefer locations near the crystal–amorphous boundary. Qualitative arguments suggested that this nonuniform distribution would persist in three dimensions. Branches that occupy a single lattice site showed a much lower tendency for segregation. To assess the validity of the prediction,

the branch distribution was studied in the present three-dimensional simulations. Figures 5–7 depict the variation of the fraction of beads that are trifunctional branch points (circles) and free branch ends (triangles), as a function of layer numbers. The horizontal dashed lines are the expectations for a completely random distribution of the short branches. Figure 5 depicts the results for a simulation in which a branch occupies a single lattice site, and Figures 6 and 7 depict results for simulations with two different amounts of the larger branch.

Attention should be directed first to the maxima in Figures 5–7. In each case, it occurs with the probability for a branch end in layer 2. However, the probability at this maximum is only ~2 times larger than the expectation for a random distribution for the shorter branches (Figure 5), but it is ~3–4 times larger than this expectation for the longer branches (Figures 6 and 7). The tendency for segregation of a branch end in layer 2 is larger for the longer branch. Examination of the profiles on all 15 layers supports the greater tendency for segregation in the longer branches. In Figures 6 and 7, there is an easily recognized change from an excess of short branches in layers 2–5 to a deficit of short branches in layers 6–15. In contrast, the pattern over layers 3–15 in Figure 5 is chaotic and provides little support for segregation of the shorter branches. No segregation of short branches *within* a layer is observed in any of the simulations.

The earlier simulations on the two-dimensional square lattice also found a strong tendency for segregation of the longer branch and a nearly random distribution for the shorter branch.[8] Comparison of the simulations in the presence of the longer branch shows that the expansion from the square to the cubic lattice produces two subtle changes. First, the distribution of short branches is much more strongly peaked in layer 2 when the simulation is performed on the square lattice. The ratio of the probabilities in layers 2 and 3 is ~3 on the square lattice, but it is nearly 1 on the cubic lattice. Second, the patterns for the branch ends and trifunctional branch points are more nearly identical on the square lattice than on the cubic lattice. In two dimensions, the short branches strongly prefer an orientation in which the trifunctional branch point and the two beads in the branch are all in layer 2. The branches have greater access to alternative conformations when the simulation moves to the cubic lattice.

The distribution of the branches in the portion of the amorphous region that is closest to the crystal–amorphous boundary arises from the interaction of two distinct affects. The first affect is the inability of the crystalline lattice to accommodate short branches that are larger than methyl.[12,19–21] Forced incorporation of these short branches in the crystal would be accompanied by severe repulsive steric interactions. These interactions are responsible for an enthalpic drive for the exclusion of the short branches from the crystal. This enthalpic drive does not demand that the branches reside in that portion of the amorphous region that is adjacent to the crystal–amorphous boundary; it only demands that they occur somewhere in the amorphous region. The present simulation includes this affect but in an indirect manner. Our simulation does not specifically look at the crystalline regions because it is assumed that branches are not found there.

The second affect is the one that is documented in the present simulation of the amorphous region between the crystalline lamellae. The conformational entropy of the amorphous region is lower if the short branches are distributed randomly throughout this region than it is when the short branches occur near the crystal–amorphous boundary. The segregation depicted in Figures 6 and 7 must be of entropic origin because the present simulations contain no energetic terms. The "solvation" of the short branches by the amorphous linear chains is accompanied by a decrease in the conformational entropy of those chains.[8] For this reason, the amorphous region attempts an exclusion of the short branches. It does so by driving them to the "surface", i.e., to the crystal–amorphous boundary.

Entangled Loops. Entanglement of loops originating from opposite crystal faces was measured by using the algorithm developed by Lacher et al.[14–16] The average link density was found to be very small (~0.02) in simulations without branches and with branches that occupy two lattice sites, indicating that the short branches do not have a significant effect on the entangled loops. Entangled loops were not examined in the simulation with the shorter branch.

This result is quite different from that reported by Lacher and Bryant.[16] They find a significant increase in the link density with initial increase in branch content. Their method does not take into account the intermolecular interactions that occur near the crystal–amorphous boundary and the segregation of short branches that is depicted in Figures 6 and 7.

Implications for Bulk Properties. The results from these simulations have several implications for the bulk properties of ethylene–1-alkene copolymers. The most important changes are in the anisotropic interfacial region, which is the preferred location for the short branches. The fractions of tie chains and entangled loops do not change greatly and therefore do not seem to be major contributor toward an increase in the tensile and tear strengths of these copolymers.

Conclusions

Three-dimensional simulations confirm the most important observations from earlier two-dimensional simulations. The major changes produced by short branches are associated with the anisotropic interfacial region. The anisotropic interfacial region grows with an increase in content of short branches that occupy two lattice sites. A branch occupying two lattice sites prefers a location in close proximity to the crystal–amorphous boundary. The distribution of short branches penetrates somewhat further into the amorphous region than was the case in the two-dimensional simulation. Some loops originating from opposite crystal faces do show entanglements, but the number of entanglements is not significantly affected as one goes from the unbranched state to the branched state. There is a slight increase in the fraction of tie chains at 2% branch content.

Acknowledgment. This research was supported by National Science Foundation Grant DMR 86-96071 and a grant from the Petroleum Research Fund, administered by the American Chemical Society.

References and Notes

(1) James, D. E. *Encycl. Polym. Sci. Eng.* **1988**, *6*, 429.
(2) Flory, P. J. *J. Am. Chem. Soc.* **1937**, *59*, 241.
(3) Flory, P. J. *J. Am. Chem. Soc.* **1947**, *69*, 2893.
(4) Axelson, D. E.; Levy, G. C.; Mandelkern, L. *Macromolecules* **1979**, *12*, 41.
(5) Mattice, W. L.; Stehling, F. C. *Macromolecules* **1981**, *14*, 1479.
(6) Usami, T.; Takayama, S. *Macromolecules* **1984**, *17*, 1756.
(7) Mathur, S. C.; Mattice, W. L. *Macromolecules* **1987**, *20*, 2165.
(8) Mathur, S. C.; Mattice, W. L. *Macromolecules* **1988**, *21*, 1354.
(9) DiMarzio, E. A.; Guttman, C. M.; Hoffman, J. D. *Polymer* **1981**, *21*, 1379.
(10) Guttman, C. M.; DiMarzio, E. A.; Hoffman, J. D. *Polymer* **1981**, *21*, 1466.

(11) Guttman, C. M.; DiMarzio, E. A.; Hoffman, J. D. *Polymer* **1982**, *22*, 525.
(12) Alamo, R.; Domszy, R.; Mandelkern, L. *J. Phys. Chem.* **1984**, *88*, 6587.
(13) Stein, R. S., personal communication.
(14) Lacher, R. C.; Bryant, J. L.; Howard, L. N.; Sumners, D. W. *Macromolecules* **1986**, *19*, 2639.
(15) Lacher, R. C.; Bryant, J. L.; Howard, L. N. *J. Chem. Phys.* **1986**, *85*, 6147.
(16) Lacher, R. C.; Bryant, J. L. *Macromolecules* **1988**, *21*, 1184.
(17) Mansfield, M. L. *Macromolecules* **1983**, *16*, 914.
(18) Flory, P. J. *Proc. Natl. Acad. Sci. U.S.A.* **1982**, *79*, 4510.
(19) Voigt-Martin, I. G.; Alamo, R.; Mandelkern, L. *J. Polym. Sci., Polym. Phys. Ed.* **1986**, *24*, 1283.
(20) Vander Hart, D. L.; Perez, E. *Macromolecules* **1986**, *19*, 1902.
(21) France, C.; Hendra, P. J.; Maddams, W. F.; Willis, H. A. *Polymer* **1987**, *28*, 710.

Determination of Propagation Rate Constants Using a Pulsed Laser Technique

Thomas P. Davis and Kenneth F. O'Driscoll*

Department of Chemical Engineering, University of Waterloo, Waterloo, Ontario, N2L 3G1 Canada

Mark C. Piton and Mitchell A. Winnik

Department of Chemistry, Lash Miller Laboratories, University of Toronto, Toronto, Ontario, M5S 1A1 Canada. *Received October 4, 1988; Revised Manuscript Received January 3, 1989*

ABSTRACT: Propagation rate constants (k_p) for the polymerization of methyl methacrylate (MMA) and styrene (STY) were determined by using a recently developed experimental technique. The procedure utilized a pulsed laser UV light source for the polymerization, and gel permeation chromatography (GPC) was used to analyze the products. The average k_p values obtained were 294 ± 9 and 78 ± 6 L mol^{-1} s^{-1} for MMA and STY, respectively at 25 °C. These k_p values were found to be independent of chain length (ν), initiator type, and concentration. The inclusion of methanol, ethylbenzene (to STY), ethyl acetate (to MMA), or poly-STY at 0.5% w/v as additive to the polymerization mixture had no significant effect on k_p.

Introduction

Recently Olaj and co-workers[1-3] have developed a technique which utilizes a pulsed laser light source to evaluate individual kinetic rate constants in free-radical polymerization. The adoption of the laser technique simplifies the kinetic expressions normally associated with nonstationary experimental procedures, e.g., rotating sector and spatially intermittent polymerization.[4]

Olaj, Bitai, and Gleixner[1] have derived the rate expression given by

$$\frac{R_p t_f}{[M]} = \frac{k_p}{k_t} \ln\left\{1 + \frac{\rho k_t t_f}{2}\left[1 + \left(1 + \frac{4}{\rho k_t t_f}\right)^{1/2}\right]\right\} \quad (1)$$

where R_p, k_p, k_t, and [M] have their usual meanings; t_f is the dark time between flashes; and ρ is the radical concentration. This relationship may be used to obtain k_p/k_t values in an analogous procedure to the rotating sector experiment.

In a later publication[2] Olaj et al. describe a technique whereby k_p can be easily determined without reference to k_t or ρ. An analysis of the molecular weight distribution by GPC of the polymer produced by such a polymerization allows calculation of ν_p, the chain length of polymer formed between successive pulses. k_p can then be obtained from

$$\nu_p = k_p[M]t_f \quad (2)$$

The process is shown schematically in Figure 1. The radical concentration generated by each pulse decays according to a second-order rate law. When the next flash occurs there is a rapid increase in the overall radical concentration and any residual radicals (from the preceding pulse) are subject to a vastly increased probability of termination. Thus formation of polymer of chain length ν_p is favored. Clearly some radicals will survive to produce polymer chains of length $2\nu_p$, $3\nu_p$, etc.

Olaj and co-workers[2] have reported a value of k_p for styrene at 25 °C as 107 L mol^{-1} s^{-1}, measured at a ν_p of 2740. More recently[3] they have amended this value to 80 L mol^{-1} s^{-1} on the basis of a reevaluation of data.

The object of the present paper is to report some experimental results obtained here by this technique, for both STY and methyl methacrylate (MMA) homopolymerizations with particular reference to the existence of any chain length effects. Similar experiments conducted on the copolymerization of STY with MMA have been described elsewhere.[6]

Experimental Section

Materials. STY and MMA were washed with aqueous sodium hydroxide, dried over calcium hydride, and distilled in an atmosphere of nitrogen under reduced pressure. Benzoin (BZ) and azobis(isobutyronitrile) (AIBN) were recrystallized three times from ethanol and methanol, respectively. Ethyl acetate (EA), ethyl benzene (EB), and methanol (MeOH) were distilled prior to use. Tetrahydrofuran (THF) for GPC measurements was refluxed over potassium, distilled, and stabilized with 2,6-di-*tert*-butyl-*p*-cresol. Poly-STY of molecular weight $M_n = 2.75 \times 10^6$ and narrow polydispersity ($M_w/M_n = 1.04$) was used as an additive in several polymerizations.

Polymerizations. The relevant freshly distilled monomer, together with initiator and additive (total volume 2 mL), was charged to Pyrex ampules (square cells 1 cm × 1 cm) and subsequently degassed and sealed.

The experimental setup used to irradiate the cells is indicated in the schematic shown in Figure 2. Each cell was placed in a thermostated cell holder maintained at 25 °C as monitored by a thermocouple.

* To whom correspondence should be addressed.

0024-9297/89/2222-2785$01.50/0